Theoretical microbubble dynamics in a viscoelastic medium at capillary breaching thresholds

Brandon Patterson[a)]
Department of Mechanical Engineering, University of Michigan, 1231 Beal Avenue, Ann Arbor, Michigan 48109

Douglas L. Miller
Department of Radiology, University of Michigan, 1301 Catherine Street, Ann Arbor, Michigan 48109

Eric Johnsen
Department of Mechanical Engineering, University of Michigan, 1231 Beal Avenue, Ann Arbor, Michigan 48109

(Received 10 June 2012; revised 1 October 2012; accepted 5 October 2012)

In order to predict bioeffects in contrast-enhanced diagnostic and therapeutic ultrasound procedures, the dynamics of cavitation microbubbles in viscoelastic media must be determined. For this theoretical study, measured 1.5 to 7.5 MHz pulse pressure waveforms, which were used in experimental determinations of capillary breaching thresholds for contrast-enhanced diagnostic ultrasound in a rat kidney, were used to calculate cavitation nucleated from contrast agent microbubbles. A numerical model for cavitation in tissue was developed based on the Keller-Miksis equation (a compressible extension of the Rayleigh-Plesset equation for spherical bubble dynamics), with a Kelvin-Voigt constitutive relation. From this model, the bubble dynamics corresponding to the experimentally obtained capillary breaching thresholds were determined. Values of the maximum radius and temperature corresponding to previously determined bioeffect thresholds were computed for a range of ultrasound pulses and bubble sizes for comparison to inertial cavitation threshold criteria. The results were dependent on frequency, the gas contents, and the tissue elastic properties. The bioeffects thresholds were above previously determined inertial cavitation thresholds, even for the tissue models, suggesting the possibility of a more complex dosimetry for capillary injury in tissue.
 [http://dx.doi.org/10.1121/1.4763993]

PACS number(s): 43.35.Ei, 43.35.Wa [CCC] Pages: 3770–3777

I. INTRODUCTION

Cavitation-bubble collapse has been a topic of interest in physical acoustics for nearly a century and has been the object of many experimental and theoretical studies, which have outlined the complexity of the phenomenon (Leighton, 1997). This field made a landmark contribution to non-ionizing radiation biology in medicine in the 1980s when the possibility of inertial cavitation, with potential induction of bioeffects, from diagnostic ultrasound pulses was predicted theoretically (Flynn, 1982; Apfel, 1982). This possibility was included in considerations for the regulation of the ultrasound output of diagnostic machines. Apfel and Holland (1991) performed detailed calculations of the response of different nuclei sizes in the form of free air microbubbles and found that the optimum size decreased with increasing frequency, f. In addition, the rarefactional pressure amplitude threshold, p, for inertial cavitation was determined for the optimum nuclei using the criterion of a >5000 K gas temperature at collapse. For nuclei in blood, the ratio of $p^{1.67}/f$ was found to have a constant value of 0.13 at the threshold, using units of MPa and MHz. This finding was used to create a Mechanical Index (MI) for regulatory purposes and for display on the screens of diagnostic ultrasound machines. The MI was set equal to the peak rarefactional pressure amplitude (PRPA) adjusted for attenuation, and divided by the square root of frequency. The regulatory guideline limit for diagnostic ultrasound was considered according to the Medical Device Amendment Act of 1976 and the maximum value existing at that time. This guideline limit was eventually set from measurements on a single diagnostic ultrasound probe to be 1.9 (Nyborg, 2001). It is noteworthy that the critical value corresponding to the Apfel and Holland (1991) result would be $p/f^{0.6} = 0.29$, which is much less than the MI limit. This discrepancy does not appear to be of concern for normal diagnostic ultrasound from both experimental (Carstensen *et al.*, 2000) and theoretical (Church, 2002) considerations.

To improve diagnostic information in ultrasound examinations, ultrasound contrast agents (UCAs) were invented. The contrast agents consist of a suspension of stabilized gas-filled microbubbles, which provide strong echoes from blood and improve contrast in sonography (Averkiou *et al.*, 2003; Raisinghani *et al.*, 2004). Soon after contrast-enhanced diagnostic ultrasound was developed, microscale bioeffects were reported (Miller *et al.*, 2008a). The typical bioeffect seen in mesentery, muscle, heart, and kidney was capillary rupture, which appeared to be caused by cavitation nucleation in blood from the circulating contrast microbubbles. Recently, the hemorrhage of glomerular capillaries was studied in a rat

a)Author to whom correspondence should be addressed. Electronic mail: awesome@umich.edu

kidney to determine PRPA thresholds and the frequency dependence of the thresholds (Miller *et al*., 2008b). Presumably, the thresholds correspond to the action of the optimum cavitation nuclei, and this approach therefore provides a means to directly compare cavitation theory with the bioeffect experiments. Over the 1.5 to 7.5 MHz frequency range tested, the thresholds were proportional to the frequency, such that *p*/*f* was approximately constant at 0.49 MPa/MHz for actual diagnostic ultrasound and 0.62 MPa/MHz for diagnostic ultrasound simulated by a laboratory pulsed-ultrasound system. These thresholds fell below the MI = 1.9 level, especially for the lower frequencies but above the inertial cavitation thresholds of Apfel and Holland (1991), and the frequency dependence was different. Evidently the bioeffect thresholds depend on cavitation dynamics not specifically tied to the inertial cavitation threshold of free air bubbles in blood determined by Apfel and Holland (1991). The fundamental reason for these results remains uncertain, which revives the non-ionizing radiation biology problem of ultrasonic cavitation in medical ultrasound.

The theoretical model of Apfel and Holland (1991) applies to air microbubbles in a Newtonian liquid. However, contrast agents in the blood stream do not necessarily exhibit such properties. It is well-known that human tissue behaves in a viscoelastic fashion (Frizzell *et al*., 1976; Madsen *et al*., 1983). The bubble dynamics greatly depend on not only the viscoelastic properties (Allen and Roy, 2000a; Yang and Church, 2005) for a given model but also on the type of model (Johnsen and Hua, 2012) and on nonlinearity (Allen and Roy, 2000b). Furthermore, the gas contained in contrast agents is not air; for example, perfluoropropane (PFP, C_3F_8) in Definity (Perflutren Lipid Microsphere, Lantheus Medical Imaging, North Billerica, MA), which may affect the collapsed temperature. The stabilizing skin or shell may not be an important factor for the capillary rupture bioeffect because the nucleation process appears to liberate a free gas microbubble. The thresholds for this cavitational bioeffect are above the destabilization threshold of the optimal microbubbles, which therefore may be modeled as free microbubbles (Sboros *et al*., 2002; Marmottant *et al*., 2005). Basically, at low PRPAs the stabilization is lost, which releases a free microbubble, thus nucleating cavitation, followed by dissolution at the conclusion of the pulse (Porter *et al*., 2006). In the case of diagnostic ultrasound, the microbubble is subjected to a series of pulses that start low, build to a peak, and finally decline. Thus, when the peak pulse arrives to cause the injury, the microbubbles likely are already destabilized.

The detailed mechanism by which cavitation causes bioeffects is unknown, although several have been proposed, such as shock emission upon collapse, growth beyond a given size, high temperatures generating free radicals, and re-entrant jets in non-spherical collapse (Nyborg *et al*., 2002). In order for such phenomena to occur, it is expected that inertial cavitation occurs. From this observation, prior studies have used the threshold for inertial cavitation as a surrogate for bioeffects (Yang and Church, 2005). This inertial cavitation threshold was developed theoretically for bubble dynamics in water (Flynn, 1975). In this work, we show that the bioeffects threshold is different from previously developed inertial cavitation thresholds. The difference between the inertial cavitation threshold calculated for air microbubbles in blood and the capillary rupture thresholds is likely due to an incomplete model. That is, the homogeneous model results may correlate better with the bioeffect results if tissue elasticity, gas contents, pulse parameters, and possibly other factors are considered.

In the current work, a different approach combining experiments and numerical modeling to studying bioeffects is followed. *In vivo* experiments were performed to determine the pulse amplitude and frequency under which bioeffects occur (Miller *et al*., 2008b). Given these experimental pulses, bubble dynamics are modeled numerically over the entire waveform duration, which is not taken into account by Apfel and Holland (1991), to determine how the bubble response correlates with the observation of bioeffects. A detailed description of the methodology is presented. The experimental setup and numerical model are first discussed in Sec. II. The results from the combined experimental and numerical procedure are presented in Sec. III. The ability of established inertial cavitation thresholds and general cavitation parameters to predict bioeffects is discussed. The article ends with a summary of the results and considerations for future work on this topic.

II. MATERIALS AND METHODS

A. Experimental setup

In a previous study of glomerular capillary hemorrhage in rats by Miller *et al*. (2008b), bioeffect thresholds were determined for ultrasound exposure with diagnostic ultrasound machines and with a laboratory system setup to simulate diagnostic scanning. The ultrasonic waveforms (pressure vs time) used for the driving pressure in this study were based on the laboratory system bioeffect thresholds at 1.50, 2.25, 3.50, 5.00, and 7.50 MHz (with corresponding bioeffect thresholds of 0.98, 1.31, 2.38, 2.82, and 6.00), which allowed more flexibility in producing the desired pulse waveforms than the diagnostic ultrasound machine.

The experiment was designed to simulate worst-case-scenario clinical conditions for CEUS. Anesthetized rats were held in place in a 75 L bath of 37 °C degassed water and exposed to ultrasound while receiving a constant 10 μl/kg/min infusion of UCA. The ultrasound probe was placed such that its focal zone was at the cortex of the right kidney. The ultrasound system consisted of a transducer, power amplifier (A-500, Electronic Navigation Industries, Rochester, NY), and a function generator (model 3314 A function generator, Hewlett Packard Co., Palo Alto, CA). Five damped single element transducers (Panametrics, Olympus NDT Inc., Waltham, MA) with 1.9 cm diameter and 3.8 cm focus were used at their resonant ultrasonic frequencies in a warmed water tank. The function generator was set using the *n*-cycle mode with $n = 3$ to produce a simple pulse train with pulse durations and PRPAs the same as used for the *in vivo* exposures. The waveforms were measured with a calibrated PVDF bilaminar film hydrophone with 0.4 mm spot size (model 805, Sonora Medical Systems, Longmont, CO) and were adjusted to equal the threshold at each frequency and to several 3 dB

increments above and below the threshold. The purpose of the progressive steps was to help identify any specific cavity behavior, which recurred at each frequency as the threshold was crossed. The hydrophone measured the alternating pressure including the PRPA, to which the constant atmospheric pressure must be added to obtain the total pressure. The highest PRPA available for the higher frequencies was limited by the transducers. The experimental waveforms are imported into MATLAB, and smoothened using a moving-average low-pass filter. This procedure results in waveforms, such as that shown in Fig. 1 for the threshold at 7.5 MHz, in which the high-frequency experimental noise is removed. The smoothened waveforms are then input into the bubble dynamics code as the driving pressure.

B. Bubble dynamics model

The bubble dynamics are modeled under the assumption that a single spherical gas bubble is subjected to a far-field pressure change (ultrasound pulse) in an infinite medium of uniform properties. Given that bioeffects are observed in some of the experiments and that it is likely that inertial cavitation occurs, it is expected that compressibility of the surrounding medium matters. Furthermore, tissue is expected to behave in a viscoelastic fashion. To account for all of these elements, the Keller-Miksis equation (Keller and Miksis, 1980), a compressible extension of the Rayleigh-Plesset equation, is considered, and the constitutive relation between the stresses and strains follows a Kelvin-Voigt viscoelastic model, as in Yang and Church (2005). Thus the nondimensional equations governing the bubble dynamics are

$$\left(1-\frac{\dot{R}}{C}\right)R\ddot{R}+\frac{3}{2}\left(1-\frac{\dot{R}}{3C}\right)\dot{R}^2 = \left(1+\frac{\dot{R}}{C}\right)\left[p_B-1-p_a-\frac{R}{C}\frac{dp_a}{dt}\right]+\frac{R}{C}\dot{p}_B,$$

where $R(t)$ is the bubble radius, C is the dimensionless sound speed, p_a is the time-varying component of the far-field pressure, and the dot represents material (time) derivatives. The bubble pressure p_B is given by

$$p_B=\left(1+\frac{2}{\mathrm{We}}\right)\frac{1}{R^{3\gamma}}-\frac{2}{\mathrm{We}R}+\tau_R, \tag{1}$$

where We is the Weber number (dimensionless surface tension), γ is the specific heat ratio for the gas, and τ_R is the normal component of the shear stress in the r-direction evaluated at $r=R$.

As in Yang and Church (2005), the Kelvin-Voigt model is used as the constitutive relation between the stresses and strains

$$\tau_R=-\frac{4}{3\mathrm{Ca}}\left(1-\frac{1}{R^3}\right)-\frac{4}{\mathrm{Re}}\frac{\dot{R}}{R}, \tag{2}$$

where Re is the Reynolds number (dimensionless viscosity), and Ca is the Cauchy number (dimensionless elasticity). The dimensionless numbers are defined in Table I. The resulting system of equations is solved for the bubble radius using a fifth-order accurate Cash-Karp Runge-Kutta method with adaptive time-step control. In the problem under consideration, the pressure pulse is smooth and its wavelength is on the order of 1 mm. Since the bubbles are initially in the micron range and do not grow beyond a few initial radii, the present Rayleigh-Plesset-type approach is justified.

The base values for tissue properties, listed in Table I, are taken from the literature (Apfel and Holland, 1991; Yang and Church, 2005). In the present work variables are nondimensionalized using a tissue density of $\rho=1000\,\mathrm{kg/m^3}$, a characteristic speed given by $u=\sqrt{p_{\mathrm{atm}}/\rho}$, where p_{atm} is atmospheric pressure, and a characteristic equilibrium radius of $R_0=1$ μm. The resulting time scale is thus close to the Rayleigh collapse time. A range of equilibrium radii within 0.1 to 2.0 μm, a typical size distribution for UCAs, is considered. Thus, changing the equilibrium radius modifies the nondimensional parameters. The specific heat is taken as $\gamma=1.13$ for PFP. Reported values of tissue elasticity fall in the 1 to 100 kPa range (Arda *et al.*, 2011). However, it is known that the elasticity may increase up to the MPa range at high strains (Krouskop *et al.*, 1998). Here, $G=100$ kPa is a nominal shear modulus (which we will subsequently refer to as elasticity) that will be considered as the base case.

Since the thresholds for cavitational bioeffects are above the destabilization threshold, the microbubbles are modeled as free bubbles (Sboros *et al.*, 2002; Marmottant *et al.*, 2005), i.e., UCA stabilizing films and shells are neglected. Additionally, the detailed effect of the physical constraint imposed by blood vessel walls is considered by including it in the bulk elasticity of the tissue. Though non-spherical perturbations may occur due to the local heterogeneity of tissue

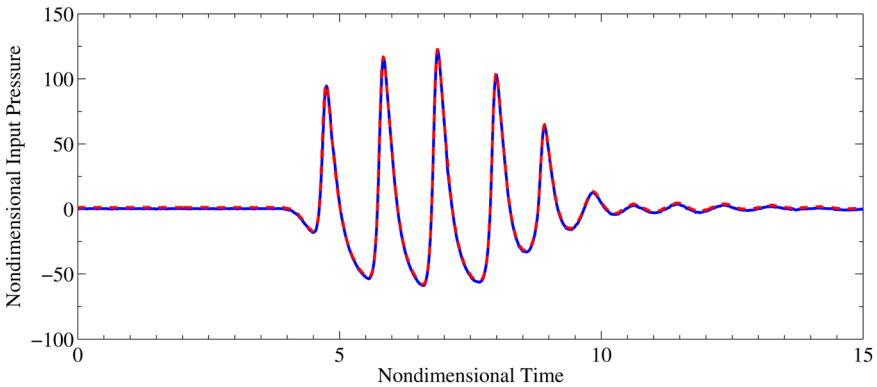

FIG. 1. (Color online) Experimental and numerical (filtered) pressure waveforms for the 7.5 MHz pulse at the threshold (peak negative pressure: 6.0 MPa, 543 ns duration, $\mathrm{MI_{eq}}=\mathrm{PRPA}/f^{1/2}=2.2$). Solid: Experimental; dashed: Numerical.

TABLE I. Base physical parameters representative of soft tissue used in the present study.

Parameter	Dimensional value	Dimensionless number
Viscosity	$\mu = 0.015$ (Pa s)	$\mathrm{Re} = \rho u R_o/\mu = 2/3$
Elasticity	$G = 10^5$ (Pa)	$\mathrm{Ca} = \rho u^2/G = 1.0$
Surface tension	$S = 0.056$ (N/m)	$\mathrm{We} = \rho u^2 R_o/S = 2$
Sound speed	$c = 1570$ (m/s)	$C = c/u = 157$

and thus lead to a significant change in the bubble dynamics, non-spherical collapse is expected to produce lower temperatures and pressures (Johnsen and Colonius, 2009). In this sense, the spherically symmetric model represents a worst-case scenario useful in determining safe, conservative parameters for CEUS procedures.

III. RESULTS AND DISCUSSION

A. Bubble response

Typical bubble responses are first shown to provide a qualitative understanding of the physics. Figures 2–4 show the history of the dimensionless bubble radius produced by a given pressure waveform for a range of essentially linear to nonlinear cases, and different elasticities (5 kPa, 100 kPa, and 1 MPa). In the linear case, the bubble oscillations are in phase with the pressure waveform. Increasing the elasticity leads to larger oscillation amplitudes, though the changes are small. At intermediate frequency and amplitude, the oscillations become larger and more nonlinear for larger elasticities. This observation, although seemingly counterintuitive, is consistent with the results of Johnsen and Hua (2012), who showed analytically that the damping of the oscillations is smaller in this range of elasticity. In the fully nonlinear case (large pulse amplitude and frequency), the oscillation amplitude becomes yet larger, thus yielding a larger maximum radius and a very small minimum radius. For all elasticities, the initial behavior is similar up to the second maximum radius. Thereafter, the stiffer case ($G = 1$ MPa) departs and collapses violently, while the other cases rebound. The maximum radius is achieved at approximately the same time in all cases, after the peak positive pressure. In all the simulations, the oscillations damp out rapidly after the passage of the pulse.

In the results of Secs. III B–III E, the maximum dimensionless radius, $R_{\max}$, and dimensional bubble temperature at collapse, $T_{\max}$, obtained using the ideal gas law, are determined by recording their largest value over the simulation. These quantities are compared to the inertial cavitation thresholds used by Apfel and Holland (1991) and Yang and Church (2005): $R_{\max} = 2$ and $T_{\max} = 5000$ K. The dependence of the bubble dynamics on the pulse amplitude, initial bubble size (i.e., UCA size distribution), pulse frequency, and tissue properties are considered individually.

B. Dependence on the pulse amplitude

Given the strong dependence of the MI on the rarefactional pressure amplitude, the influence of the pulse amplitude on the bubble dynamics is first evaluated. Figure 5 shows the dimensionless maximum radius as a function of rarefactional pressure amplitude. Initial bubble radii ranging between 0.1 and 2.0 μm are shown, as well as different frequencies. The open symbols denote cases where bioeffects did not occur, while the filled symbols denote the occurrence of bioeffects.

The results show that the bubble dynamics, through the maximum radius, scale with the pulse amplitude. Although the results do not collapse fully onto a line, a general trend is discernible. At low amplitude, the increase in the maximum radius is approximately linear; beyond some amplitude, the bubble undergoes nonlinear oscillations, thus explaining the different depenced and larger spread. These results are consistent with the plots shown in Figs. 2–4. Over a broad range of amplitudes, the occurrence of bioeffects has little correlation with pulse amplitude alone: At a given amplitude, bioeffects may be observed or not, depending on the bubble size and pulse frequency. Only at very large pressure amplitudes (PRPA > 4.20 MPa) are bioeffects systematically observed regardless of the bubble size and pulse frequency. This behavior is not surprising, since at these amplitudes the bubble response is expected to be highly nonlinear. Conversely, at low amplitudes (PRPA < 0.97 MPa), the oscillations are linear and no bioeffects are observed, regardless of bubble size and pulse frequency. In this latter case, most bubbles whose $R_{\max}/R_o$ is below 2 do not exhibit bioeffects; however, this behavior depends on the value of elasticity, as shown in

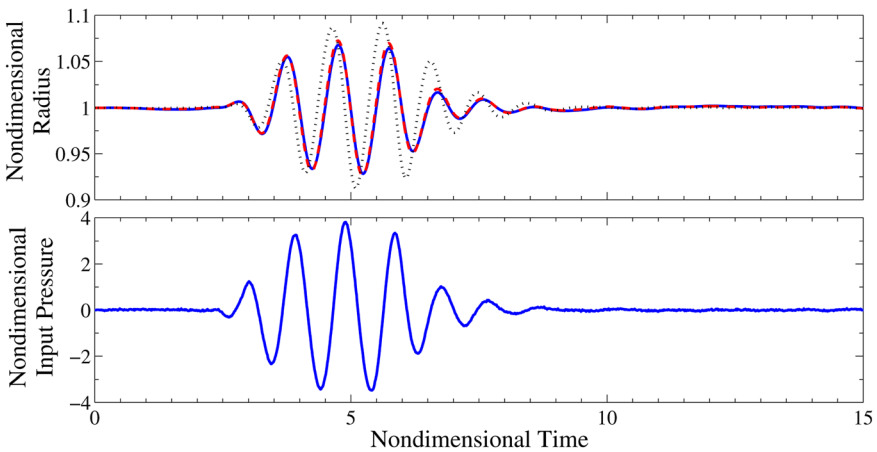

FIG. 2. (Color online) History of the bubble radius (top) and input-pressure waveform (bottom) for an essentially linear case (frequency: 1.5 MHz; peak negative pressure: 0.35 MPa). No bioeffects are observed here. $R_0 = 1$ μm; solid: $G = 5$ kPa; dashed: $G = 100$ kPa; dotted: $G = 1$ MPa.

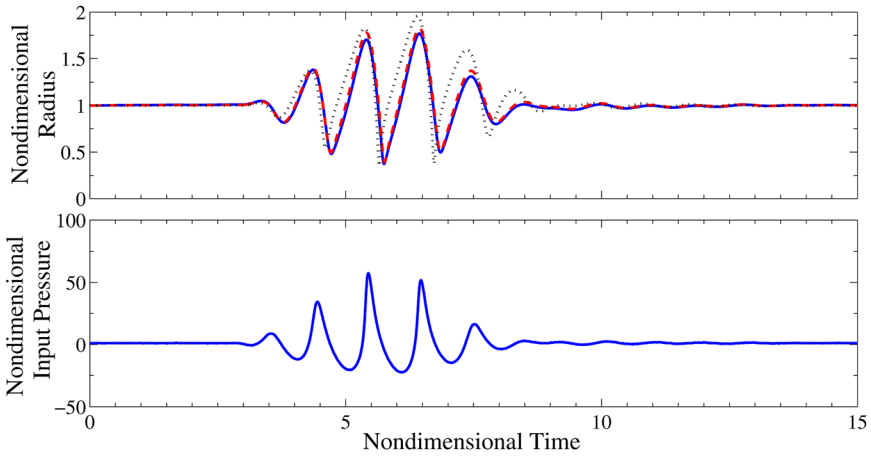

FIG. 3. (Color online) History of the bubble radius (top) and input-pressure waveform (bottom) for a moderately nonlinear case (frequency: 3.5 MHz; peak negative pressure: 2.4 MPa). Bioeffects are observed here. $R_0 = 1\,\mu$m; solid: $G = 5$ kPa; dashed: $G = 100$ kPa; dotted: $G = 1$ MPa.

Sec. III E. Although not shown here for conciseness, similar results are obtained for peak positive pressure.

Similarly, the criterion $T_{\max} > 5000$ K is not achieved with PFP. As shown in Fig. 6, the observed temperatures for PFP are far below this value, although the results for air approach it. This result is expected since the criterion was determined for air, which has a larger specific heat ratio ($\gamma_{\text{air}} = 1.4$) than PFP ($\gamma = 1.13$). The specific heat ratio appears in the internal gas pressure term in Eq. (1); its effect on the bubble dynamics is minor if the minimum radius is not very small, as in Fig. 6. Still, since the adiabatic relationships for an ideal gas are used, the temperature is significantly affected by the different specific heat ratio. Hence, even though the bubble dynamics are not strongly affected by the specific heat ratio, the maximum temperature is.

C. Dependence on the initial (equilibrium) bubble radius

In the experiment, the size distribution of the UCAs is not known exactly. It is desirable to know whether the observed bioeffects are caused by all bubbles responding to the ultrasound or whether a specific size is more likely to be responsible at the bioeffects threshold. To answer this question, for each experimental frequency, bubbles of different radii ranging from 0.1 to 2 μm are subjected to the pressure waveform corresponding to the bioeffects threshold amplitude. It should be noted that varying the equilibrium radius changes the non-dimensional parameters. Figure 7 shows the maximum dimensionless radius, for both water (zero elasticity) and tissue (finite elasticity, $G = 100$ kPa), for the amplitude at which bioeffects are first observed at a given frequency.

Excluding the smallest size, the bubble response in tissue is monotone and changes little for a given frequency; there is no initial size that consistently leads to a dramatic response. The somewhat erratic behavior of the small bubbles may imply that such sizes are not present in UCA concentrations. On the other hand, the behavior is more irregular for water, particularly at small radii: For a given frequency, there is an optimal size that exhibits the largest response; these variations are much larger than for tissue.

D. Dependence on the pulse frequency

The dependence of the bubble response on the pulse frequency is considered in this section. Figure 8 shows the maximum dimensionless and dimensional radius for all initial bubble sizes and amplitudes vs frequency. The square symbols denote cases in which bioeffects were observed in the experiments, while the circular symbols represent no bioeffects. The initial bubble sizes are not discriminated here for simplicity.

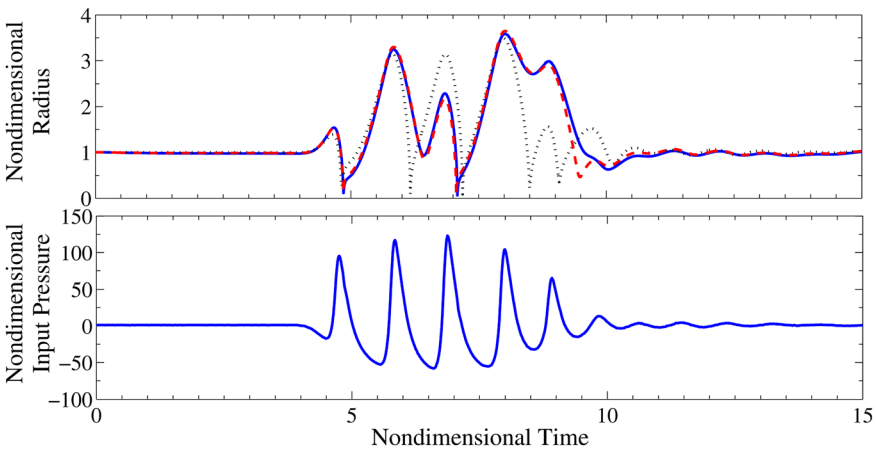

FIG. 4. (Color online) History of the bubble radius (top) and input-pressure waveform (bottom) for a highly nonlinear case (frequency: 7.5 MHz; peak negative pressure: 6.0 MPa). Bioeffects are observed here. $R_0 = 1\,\mu$m; solid: $G = 5$ kPa; dashed: $G = 100$ kPa; dotted: $G = 1$ MPa.

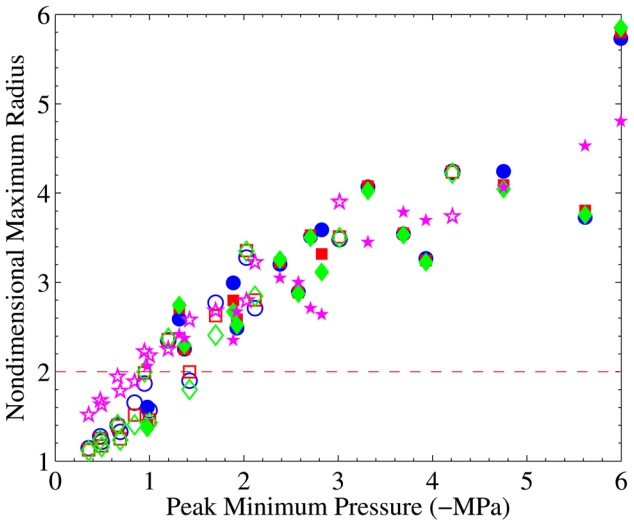

FIG. 5. (Color online) Dependence of the dimensionless maximum bubble radius on the peak negative pressure for $G = 100$ kPa. Empty symbols: No bioeffects; filled symbols: Bioeffects. Pentagrams: 0.1 μm; circles: 0.5 μm; squares: 1 μm; diamonds: 2 μm; frequency: 1.5 to 7.5 MHz.

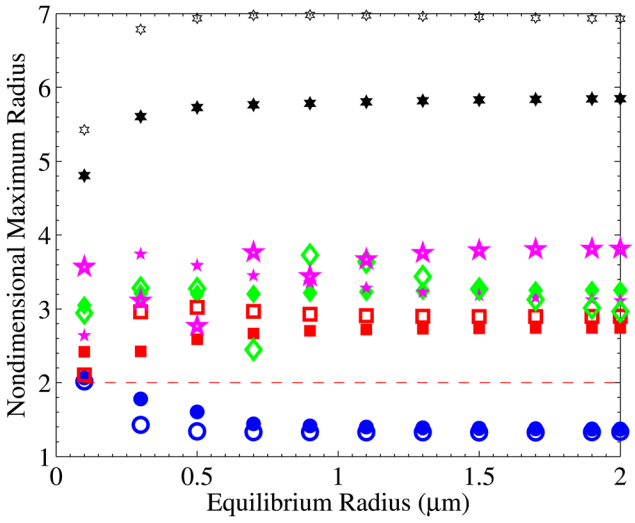

FIG. 7. (Color online) Dependence of the dimensionless maximum bubble radius on the initial bubble size for the amplitude at which bioeffects are first observed, at a given frequency, for $G = 100$ kPa. Empty symbols: Water; filled symbols: Tissue. Circles: 1.50 MHz; squares: 2.25 MHz; diamonds: 3.50 MHz; pentagrams: 5.00 MHz; hexagrams: 7.50 MHz.

With the exception of a few outliers, a clear separation between cases for which bioeffects did and did not occur is observed; in other words, the bioeffect threshold has a strong dependence on the frequency. The trend appears to be approximately linear with frequency. Large growth may be achieved with no evident bioeffects, especially at high frequencies. The quantity R_{max} is a measure of cavitation collapse since it is related to the available energy of the bubble. Thus, the present results indicate that cavitation collapse is expected to play an important role regarding bioeffects, although the precise mechanism cannot be inferred. Again, the existing criteria for inertial cavitation thresholds are frequency-independent and do not correlate well with the bioeffects threshold, which clearly shows a strong dependence on frequency.

Another hypothesis is that bubble growth may be responsible for capillary breaching. However, the plot of the dimensional maximum radius vs frequency does not show systematic bioeffects beyond a certain size, e.g., some capillary diameter. Thus, growth is not the sole mechanism by which bioeffects occur. However, the data remains inconclusive due to the inability to identify the cases in which cavitation collapse is the dominant effect.

E. Dependence on the tissue properties

As suggested in Figs. 2–4, the bubble dynamics are sensitive to the tissue properties, specifically the elasticity. However, different types of tissue may have very different properties. Many of the measurements of tissue elasticity are made *in vitro* and depend strongly on tissue preparation, storage, and degradation, as well as method of measurement.

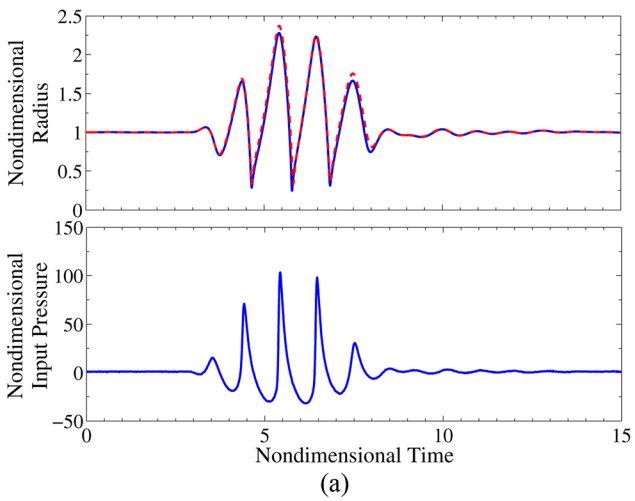

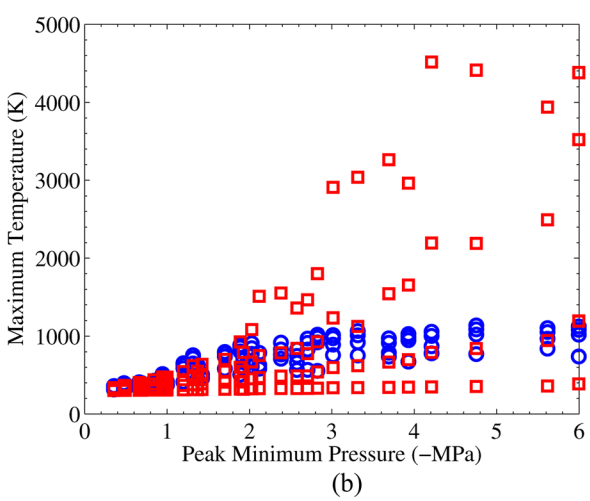

FIG. 6. (Color online) Dependence of the bubble dynamics on the gas contents ($G = 100$ kPa). (a) History of the bubble radius for PFP (solid line) and air (dashed line). $R_0 = 1$ μm; frequency: 3.5 MHz; peak negative pressure: 3.3 MPa. (b) Maximum temperature for PFP (circles) and air (squares). $R_0 = 1$ to 2 μm; frequency: 1.5 to 7.5 MHz.

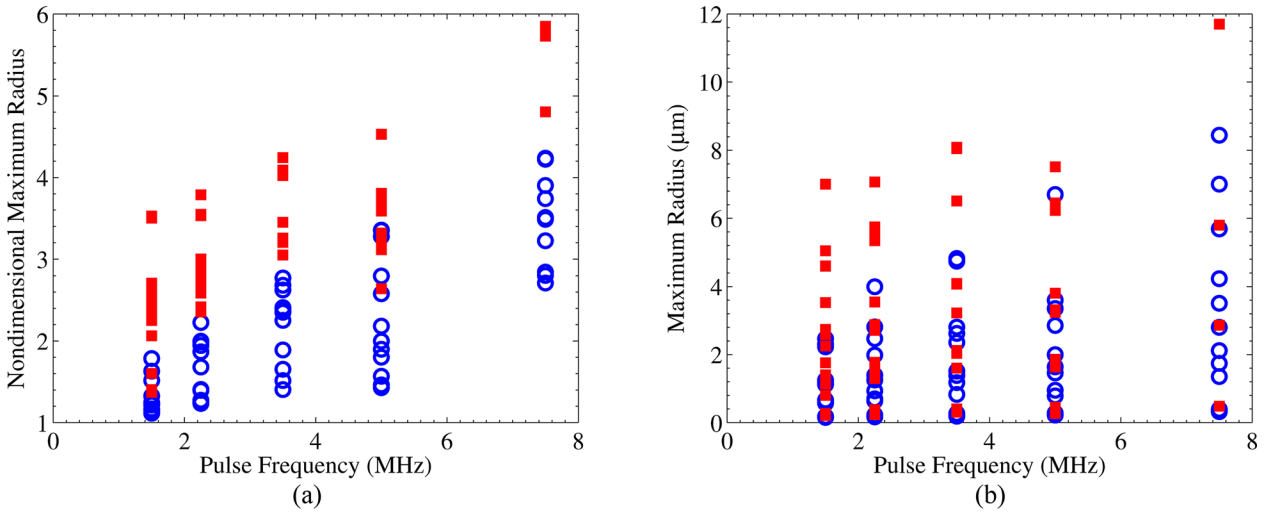

FIG. 8. (Color online) Dependence of the bubble dynamics on the frequency for $G = 100$ kPa. $R_0 = 0.1$ to 2 μm; empty circles: No bioeffects; squares: Bioeffects. (a) Dimensionless maximum bubble radius and (b) Dimensional maximum bubble radius.

Consequently, it is possible that these measurements do not accurately represent the current behavior. To explore the effect of the elasticity on the results and the correlation to bioeffects, Fig. 9 shows the maximum dimensionless radius for all initial bubble sizes and amplitudes vs frequency for $G = 5$ kPa and $G = 1$ MPa. Although seemingly high, the latter elasticity is chosen to match the work of Yang and Church (2005).

The bubble dynamics and correlation to bioeffects significantly change when reducing the elasticity. For a value of 5 kPa, the discrimination is no longer clear. The bubble dynamics are closer to the behavior in water, such that different sizes may have dramatically different responses to the same waveform, as explained previously. On the other hand, the stiffer medium ($G = 1$ MPa) shows an even sharper demarcation, which again appears to be approximately linear. Given the sensitivity of the results on the elasticity, it is clear that more precise *in vivo* data is required for elasticities of tissues at the relevant strain rates.

Although not shown here, the type of viscoelastic model significantly affects the bubble dynamics (Johnsen and Hua, 2012; Patterson *et al.*, 2012). For instance, a standard linear solid model, which includes stress relaxation in addition to elasticity, leads to very different maximum radii and oscillation properties (frequency and damping). For large relaxation times, elasticity variations become negligible.

IV. CONCLUSIONS

In the present work, a numerical model is used to investigate experimentally observed bioeffects as a result of contrast-enhanced ultrasound. This work is unique in its combination of experimental results and numerical modeling. For the experimentally generated input pressure waveforms it is known which of these triggered bioeffects, and from the numerical model we obtained calculated values for the dimensionless maximum radius and dimensional maximum

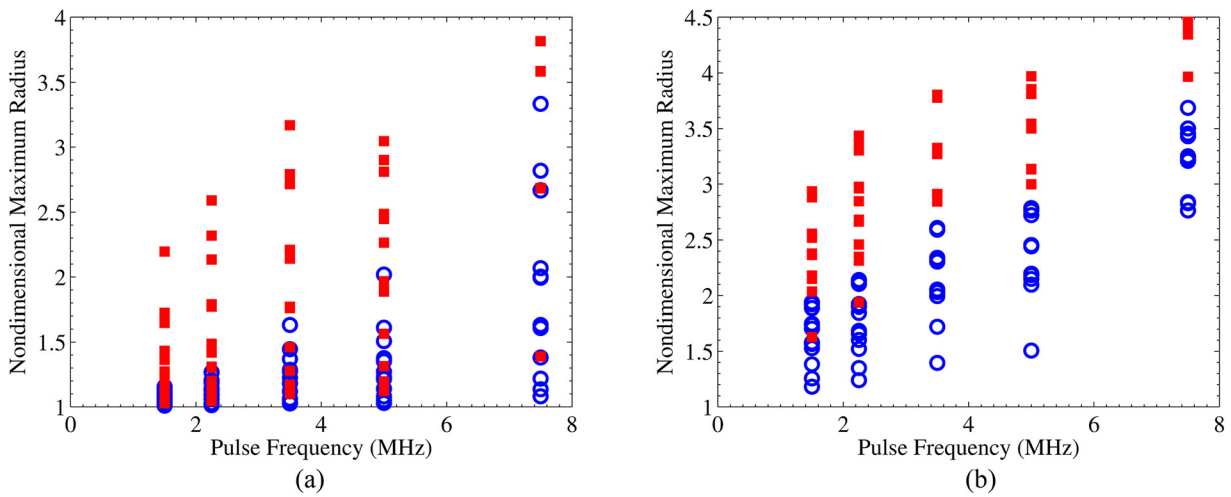

FIG. 9. (Color online) Dependence of the dimensionless maximum bubble radius on the frequency. $R_0 = 0.1$ to 2 μm; empty circles: No bioeffects; squares: Bioeffects. (a) $G = 5$ kPa and (b) $G = 1$ MPa.

temperature for each of these cases. By comparing the results of this study to previously established inertial cavitation thresholds used by Apfel and Holland (1991) and Yang and Church (2005), $T_{max} = 5000$ K and $R_{max} = 2$, it would appear that the inertial cavitation threshold does not play a role in determining the bioeffects threshold. However, it is unlikely that the inertial cavitation threshold is irrelevant. Instead, it is far more probable that these thresholds are not defined appropriately for cavitation in a viscoelastic medium, such as soft tissue. This work suggests the need for further experimental and numerical studies of cavitation in viscoelastic media.

The present work shows a strong correlation between cavitation dynamics and bioeffects when considering the pulse frequency. From the plot of maximum dimensionless radius vs frequency, there is a clear separation between when bioeffects do and do not occur, and based on these results it appears that the frequency of the input pressure waveform is of key importance to the definition of a bioeffect threshold, and likely the inertial cavitation threshold as well.

The present work shows that the elasticity of tissue significantly affects the bubble dynamics. This finding is perhaps not completely unexpected given that bubble dynamics are known to strongly depend on viscoelastic properties and the model. The present study shows the need for more accurate measurements of material properties and for determining appropriate constitutive models for soft tissue, particularly at high strain rates. Finally, although the present work suggests that inertial cavitation collapse plays an important role with respect to bioeffects, it does not shed light on the exact mechanism, e.g., shock emission upon collapse, growth beyond a given size, high temperatures generating free radicals, re-entrant jets in non-spherical collapse, etc. In future work we plan on investigating this injury mechanism by conducting direct simulations of the full equations of motion for bubble dynamics in a viscoelastic medium.

Allen, J. S., and Roy, R. A. (**2000a**). "Dynamics of gas bubbles in viscoelastic fluids. I. Linear viscoelasticity," J. Acoust. Soc. Am. **107**, 3167–3178.

Allen, J. S., and Roy, R. A. (**2000b**). "Dynamics of gas bubbles in viscoelastic fluids. II. Nonlinear viscoelasticity," J. Acoust. Soc. Am. **108**, 1640–1650.

Apfel, R. E. (**1982**). "Acoustic cavitation: A possible consequence of biomedical use of ultrasound," Br. J. Cancer Suppl. **45**, 140–146.

Apfel, R. E., and Holland, C. K. (**1991**). "Gauging the likelihood of cavitation from short-pulse low-duty cycle diagnostic ultrasound," Ultrasound Med. Biol. **17**, 179–185.

Arda, K., Ciledag, N., Aktas, E., Aribas, B. K., and Kose, K. (**2011**). "Quantitative assessment of normal soft-tissue elasticity using shear-wave ultrasound elastography," AJR, Am. J. Roentgenol. **197**, 532–536.

Averkiou, M., Powers, J., Skyba, D., Bruce, M., and Jensen, S. (**2003**). "Ultrasound contrast imaging research," Ultrasound Quart. **19**, 27–37.

Carstensen, E. L., Gracewski, S., and Dalecki, D. (**2000**). "The search for cavitation in vivo," Ultrasound Med. Biol. **26**, 1377–1385.

Church, C. C. (**2002**). "Spontaneous homogeneous nucleation, inertial cavitation and the safety of diagnostic ultrasound," Ultrasound Med. Biol. **28**, 1349–1364.

Flynn, H. G. (**1975**). "Cavitation dynamics. II. Free pulsations and models for cavitation bubbles," J. Acoust. Soc. Am. **68**, 1160–1170.

Flynn, H. G. (**1982**). "Generation of transient cavitation in liquids by microsecond pulses of ultrasound," J. Acoust. Soc. Am. **72**, 1926–1932.

Frizzell, L. A., Carstensen, E. L., and Dyro, J. F. (**1976**). "Shear properties of mammalian-tissues at low megahertz frequencies," J. Acoust. Soc. Am. **60**, 1409–1411.

Johnsen, E., and Colonius, T. (**2009**). "Numerical simulations of non-spherical bubble collapse," J. Fluid Mech. **629**, 231–262.

Johnsen, E., and Hua, C. (**2012**). "Bubble dynamics in a standard linear solid (viscoelastic) medium," in *Proceedings of the 8th International Symposium on Cavitation*, Singapore, pp. 1–5.

Keller, J. B., and Miksis, M. (**1980**). "Bubble oscillations of large amplitude," J. Acoust. Soc. Am. **68**, 628–633.

Krouskop, T. A., Wheeler, T. M., Kallel, F., Garra, B. S., and Hall, T. (**1998**). "Elastic moduli of breast and prostate tissues under compression," Ultrason. Imaging **20**, 260–274.

Leighton, T. G. (**1997**). *The Acoustic Bubble* (Academic Press, London), pp. 301–338.

Madsen, E. L., Sathoff, H. J., and Zagzebski, J. A. (**1983**). "Ultrasonic shear-wave properties of soft-tissues and tissue-like materials," J. Acoust. Soc. Am. **74**, 1346–1355.

Marmottant, P., van der Meer, S., Emmer, M., Versluis, M., de Jong, N., Hilgenfeldt, S., and Lohse, D. (**2005**). "A model for large amplitude oscillations of coated bubbles accounting for buckling and rupture," J. Acoust. Soc. Am. **118**, 3499–3505.

Miller, D. L., Averkiou, M. A., Brayman, A. A., Everbach, E. C., Holland, C. K., Wible, J. H., Jr., and Wu, J. (**2008a**). "Bioeffects considerations for diagnostic ultrasound contrast agents," J. Ultrasound Med. **27**, 611–632.

Miller, D. L., Dou, C., and Wiggins, R. C. (**2008b**). "Frequency dependence of kidney injury induced by contrast-aided diagnostic ultrasound in rats," Ultrasound Med. Biol. **34**, 1678–1687.

Nyborg, W. L. (**2001**). "Biological effects of ultrasound: Development of safety guidelines. Part II: General review," Ultrasound Med. Biol. **27**, 301–333.

Nyborg, W. L., Carson, P. L., Carstensen, E. L., Dunn, F., Miller, M. W., Miller, D. L., Thompson, H. E., and Ziskin, M. C. (**2002**). "Exposure criteria for medical diagnostic ultrasound: II. Criteria based on all known mechanisms," Report No. 140 (National Council on Radiation Protection and Measurements, Bethesda, MD).

Patterson, B., Miller, D. L., and Johnsen, E. (**2012**). "Theoretical microbubble dynamics in a homogeneous viscoelastic medium at capillary breaching thresholds," in *Proceedings of Acoustic*, Hong Kong, pp. 1–6.

Porter, T. M., Smith, D. A., and Holland, C. K. (**2006**). "Acoustic techniques for assessing the Optison destruction threshold," J. Ultrasound Med. **25**, 1519–1529.

Raisinghani, A., Rafter, P., Phillips, P., Vanna, M. A., and DeMaria, A. N. (**2004**). "Microbubble contrast agents for echocardiography: Rationale, composition, ultrasound interactions, and safety," Cardiol. Clin. **22**, 171–180.

Sboros, V., MacDonald, C. A., Pye, S. D., Moran, C. M., Gomatam, J., and McDicken, W. N. (**2002**). "The dependence of ultrasound contrast agents backscatter on acoustic pressure: Theory versus experiment," Ultrasonics **40**, 579–583.

Yang, X., and Church, C. (**2005**). "A model for the dynamics of gas bubbles in soft tissue," J. Acoust. Soc. Am. **118**, 3595–3606.